Cortical lamina-dependent blood volume changes in human brain at 7 T

Laurentius Huber[a*], Jozien Goense[b,c], Aneurin J. Kennerley[d], Robert Trampel[a], Maria Guidi[a], Enrico Reimer[a], Dimo Ivanov[e], Nicole Neef[a], Claudine J Gauthier[a], Robert Turner[a], and Harald E. Möller[a]

[a] Max Planck Institute for Human Cognitive and Brain Sciences, Leipzig, Germany
[b] Institute of Neuroscience and Psychology, University of Glasgow, Glasgow, UK
[c] Max Planck Institute for Biological Cybernetics, Tübingen, Germany
[d] Signal Processing in Neuroimaging and Systems Neuroscience, University of Sheffield, Sheffield, UK
[e] Maastricht Brain Imaging Centre, Maastricht University, Maastricht, The Netherlands

*Corresponding author:
Laurentius Huber
PhD-student, NMR Unit, Max Planck Institute for Human Cognitive and Brain Sciences
Stephanstraße 1A, 04103 Leipzig, Germany
Email: renzo@cbs.mpg.de
Phone: +49 341 9940-2427

Running Title: Layer-dependent CBV changes in humans
The body of the text contains 6830 words (without 2300 words in references)

Highlights:

- A CBV-sensitive fMRI method is developed for high resolution fMRI in humans.
- Lamina-dependent CBV fMRI responses are shown in humans.
- VASO cortical profiles are validated with Fe-contrast agent fMRI in animals.
- Sensitivity to large veins can be minimized using VASO-CBV instead of BOLD fMRI.
- Ipsilateral fMRI responses to finger-tapping are positive in M1 and negative in S1.

Abstract

Cortical layer-dependent high (sub-millimeter) resolution functional magnetic resonance imaging (fMRI) in human or animal brain can be used to address questions regarding the functioning of cortical circuits, such as the effect of different afferent and efferent connectivity on activity in specific cortical layers. The sensitivity of gradient echo (GE) blood oxygenation level dependent (BOLD) responses to large draining veins reduces its local specificity and can render the interpretation of the underlying laminar neural activity impossible. Application of the more spatially specific cerebral blood volume (CBV) based fMRI in humans has been hindered by the low sensitivity of the non-invasive modalities available. Here, a Vascular Space Occupancy (VASO) variant, adapted for use at high field, is further optimized to capture layer-dependent activity changes in human motor cortex at sub-millimeter resolution. Acquired activation maps and cortical profiles show that the VASO signal peaks in grey matter at 0.8 - 1.6 mm depth, and deeper compared to the superficial and vein-dominated GE-BOLD responses. Validation of the VASO signal change versus well-established iron-oxide contrast agent based fMRI methods in animals showed the same cortical profiles of CBV change, after normalization for lamina-dependent baseline CBV. In order to evaluate its potential of revealing small lamina-dependent signal differences due to modulations of the input-output characteristics, layer-dependent VASO responses were investigated in the ipsilateral hemisphere during unilateral finger tapping. Positive activation in ipsilateral primary motor cortex

and negative activation in ipsilateral primary sensory cortex were observed. This feature is only visible in high-resolution fMRI where opposing sides of a sulcus can be investigated independently because of a lack of partial volume effects. Based on the results presented here we conclude that VASO offers good reproducibility, high sensitivity, and lower sensitivity than GE-BOLD to changes in larger vessels, making it a valuable tool for layer-dependent fMRI studies in humans.

Abbreviations: BOLD = blood oxygenation level dependent; CBV = cerebral blood volume; CNR = contrast-to-noise ratio; CSF = cerebrospinal fluid; ΔCBV = change in CBV; EPI = echo planar imaging; Fe = iron; fMRI = functional magnetic resonance imaging; GE = gradient echo; GM = grey matter; ROI = region of interest; SNR = signal-to-noise ratio; SS-SI-VASO = slice-selective slab-inversion VASO; TE = echo time; TI = inversion time; TR = repetition time; VASO = vascular space occupancy.

Key words: vascular space occupancy, SS-SI-VASO, cerebral blood volume, cortical profiles, layer-dependent fMRI, negative BOLD response, 7 Tesla MRI

1. Introduction

Sub-millimeter spatial resolution, functional magnetic resonance imaging (fMRI) enables measurement of blood oxygen level dependent (BOLD) responses as a function of cortical depth in human and animal brains. If layer-dependent differences in neural metabolism could be inferred from high resolution fMRI responses, insight might be provided for instance, on the question, how differences in afferent and efferent connectivity affect processing in a given brain region. At these higher spatial resolutions, the fMRI contrast is dominated by thermal noise (Triantafyllou et al., 2005), rather than physiological noise, and therefore it can fully benefit from the use of the very high available field strengths, such as the widely used 7 Tesla.

Layer-dependent fMRI at high fields might therefore enable a new level of brain research, with the potential not only to detect *which* brain area is activated, but also *how* it is activated. For example, Trampel et al., (2012) investigated the increased activity in primary motor cortex (M1) associated with motor imagery as compared with an actual motion task, demonstrating that the layer dependence of the ensuing activation differs strikingly for the two conditions. In another example, layer-dependent fMRI was used to study the input characteristics of sensory cortex, and thus to investigate the restructuring of brain connectivity consequent upon denervation-induced plasticity (Yu et al., 2014). In the visual system, layer-dependent fMRI can help to address questions regarding the feedforward-feedback pathways during excitatory and inhibitory stimuli (Goense et al., 2012).

The limiting factor of such investigations in the human brain is that the noninvasive high-sensitivity fMRI modalities recording the effects of vascular changes are specific not only to the neural activity within individual cortical layers, but are also sensitive to changes in blood parameters, such as oxygenation, that propagate across the cortex. In particular, because gradient echo (GE)-BOLD signal also arises from draining veins (Turner, 2002), it may be difficult to interpret the signal unambiguously in terms of spatially specific underlying neural activity. GE-BOLD responses are weighted towards the site of relatively large pial veins, which are draining the area of activated cortex (De Martino et al., 2013; Polimeni et al., 2010).

There is evidence from animal studies, however, that relative cerebral blood volume (CBV) changes peak in deeper cortical layers, closer to the site of metabolic activity changes (Goense et al., 2012; Kennerley et al., 2005; Kim et al., 2013). The most widely used noninvasive CBV-weighted fMRI method in humans is Vascular Space Occupancy (VASO) (Huber et al., 2014a; Lu et al., 2013). It takes advantage of differences in the longitudinal relaxation time, T_1, between blood and tissue, and employs a blood-nulling inversion-recovery sequence to obtain an MR signal proportional to CBV. While invasive contrast-agent-based CBV-weighted fMRI methods have yielded promising results in animal studies, layer-dependent analysis of CBV change in humans has been precluded so far by the inherently low contrast-to-noise ratio (CNR) of VASO and other noninvasive CBV-based fMRI methods.

In this study, we present an approach to VASO-based fMRI that enables simultaneous noninvasive acquisition of CBV and BOLD signal changes at high field (7 T) in human motor cortex with sub-millimeter resolution. The cortical-depth dependence of CBV-based VASO fMRI was compared in detail with BOLD fMRI. The VASO-CBV results were validated in animal models using fMRI measures of CBV changes with established iron-oxide-based contrast agents. To elucidate the extent to which the different modalities are dominated by local surface vasculature, we compared VASO and iron-oxide-based fMRI data with GE-BOLD data, which is affected by unwanted sensitivity to large translaminar blood vessels. The final goals of this study are a) to assess whether CBV-based fMRI in humans is sensitive enough to distinguish small hemodynamic responses in tasks designed for investigation of input and output cortical layers, and b) to investigate whether our proposed high-CNR CBV-based fMRI method can overcome specificity limitations of GE-BOLD and thus allow quantitative noninvasive measurements of layer-dependent activity profiles to be used in human fMRI.

2. Materials and Methods

2.1. Challenges for high-resolution fMRI

fMRI in human brain at conventional field strengths at sub-millimeter spatial resolution suffers from inadequate CNR for the study of cortical layer dependence of brain activity. Advanced imaging technologies are thus required. Early human laminar fMRI results were typically acquired with higher in-plane resolution compared to the slice thickness (Yacoub et al., 2008) and laminar profile analysis has relied on scanning flat, relatively unsulcated grey matter (GM) regions with image slices orthogonal to the cortex (Koopmans et al., 2010; Ress et al., 2007). The use of cortical surface analysis of fMRI data acquired with isotropic resolution has helped to expand the application of layer-dependent fMRI over larger areas of folded cortex (De Martino et al., 2013; Koopmans et al., 2011; Polimeni et al., 2010; Siero et al., 2014; Siero et al., 2011; Trampel et al., 2012).

The present study considers the ‘hand-knob’ region of human primary motor cortex, which has a relatively simple and predictable folding pattern. For such a structure, it is feasible to adopt the earlier strategy of using a slice thickness greater than the in-plane resolution, with its consequent gain in CNR. This is appropriate for the use of VASO, which is a technique for scanning a limited number of slices and has somewhat lower CNR compared with BOLD.

Another critical issue in high-resolution fMRI in humans is the broadening of the point spread function in the phase-encoding direction due to the often-required longer duration of the acquisition window with respect to T_2* decay, also referred to as T_2* blurring (Hetzer et al., 2011; Kemper et al., 2014). This problem can be circumvented by the use of a small imaging matrix, which is made feasible by reducing the size of the field of view (FOV) or using a high parallel imaging acceleration factor. Since the spatial extent of the regions of interest (ROIs) of this study is on the same scale as the extent of the receive fields of individual coil elements, high acceleration tends to result in a relatively high *g*-factor penalty. Furthermore, because this study deals with relatively small predefined ROIs in M1, large areal coverage is not required. Pilot experiments showed that the highest temporal SNR (tSNR) was achieved using a selection of individual receiver coil elements in a surface-coil like fashion, without additional acceleration. Therefore, in this study small FOVs are captured without parallel imaging acceleration.

For optimized CBV-weighted signal at high fields, a Slice-Selective Slab-Inversion (SS-SI) variant of VASO is beneficial (Huber et al., 2014a). This method relies on the fact that the blood T_1 at 7 T is comparable to the refill time of the vasculature; its CNR has been shown to be approximately 60% that of BOLD at the same field strength. To circumvent the effects of inflow of 'fresh' (non-inverted) blood magnetization into the microvasculature of the imaging slice in VASO at 7 T (Hua et al., 2013), the inversion efficiency of the inversion pulse was reduced, to make the blood nulling time of the VASO sequence shorter than the arterial arrival time. This is particularly necessary in the sensory motor cortex, due to its relatively short arterial arrival time (Mildner et al., 2014). The application of a reduced inversion efficiency is associated with smaller GM signal at the blood nulling time and therefore comes at the cost of lower sensitivity. Since the CBV sensitivity of VASO relies only on the nulling of intravascular signal, and not on the absolute value of TI (Lu et al., 2013), the application of a partial inversion pulse will not affect the original VASO contrast.

2.2. Correction of BOLD contamination in VASO signal

With increasing field strength, the positive BOLD signal change during neural activation increasingly counteracts the negative VASO signal change. The GE-BOLD effect typically has two components: intravascular and extravascular. At 7 T, the extravascular BOLD dominates the intravascular BOLD by more than 90% (Uludag et al., 2009). This extravascular BOLD contamination is considerably larger than the desired VASO signal change and needs to be corrected for. In SS-SO VASO, an interleaved, pair-wise acquisition of VASO and BOLD images is used to distinguish between BOLD and VASO signal components of the resulting signal. When the pure BOLD contrast contribution is known, the BOLD contamination in the VASO image can be factored out, as described earlier (Huber et al., 2014a). In short: Both BOLD and VASO time series are expected to have the same BOLD T_2^* weighting, but different VASO T_1 weighting. Hence, when the voxel-wise ratio image between the BOLD and VASO images is formed, the T_2^* weighting is canceled out, providing BOLD-corrected VASO contrast. As long as both images are acquired with the identical EPI acquisition module, the T_2^* weighting cancels out, independently of TE and readout duration. This BOLD correction mechanism relies on the assumption that changes in BOLD weighting are slower than the time between consecutive image acquisitions. Furthermore, it assumes that extravascular effects contribute much more

to the BOLD response than intravascular effects. In this correction scheme, BOLD contaminations are considered to be solely based on changes in T_2^*. Hence, the applied correction scheme is assumed to account for BOLD contaminations in all compartments of the vascular tree including arteries, capillaries and veins. Considering that the intravascular BOLD contamination is vanishingly small at 7 T for any vessel diameter (Uludag et al., 2009), any residual intravascular BOLD contamination is considered to be negligible, independent of the cortical depth. The dynamic division of the BOLD correction scheme used here inherently corrects for all potential signal drifts, and thus tends to improve the signal stability.

2.3. CBV sensitivity in VASO and iron-oxide-based fMRI

Intravenous injection of paramagnetic intravascular contrast agents, such as iron oxide nanoparticles, affects the extravascular water signal in proportion to the CBV (Mandeville, 2012). The normalized iron-oxide-based signal can be written as:

$$\frac{S(d)}{S(d=0)} = e^{-k(d)CBV}, \quad \text{Eq. 1}$$

where CBV is the relative blood volume per volume of tissue in units of ml/100ml, *k(d)* is a function of contrast-agent dose, *d*, its susceptibility difference from the surroundings, the echo time, TE, and field strength (Kim et al., 2013; Tropres et al., 2001). In order to avoid potential contamination by BOLD changes to the tissue susceptibility, *S(d)*, and *S(d = 0)* should refer to the same activation state (rest or activity). Functional iron-oxide-based signal change can be written as:

$$\frac{\Delta S}{S_{rest}} \approx \frac{e^{-k(d)CBV_{act}} - e^{-k(d)CBV_{rest}}}{e^{-k(d)CBV_{rest}}} \approx -\frac{\Delta CBV}{CBV_{rest}}, \quad \text{Eq. 2}$$

with $\Delta CBV = CBV_{act} - CBV_{rest}$ and assuming that $k(d) \ll CBV_{rest}$. In contrast, VASO signal change can be described as (Lu et al., 2013):

$$\frac{\Delta S}{S_{rest}} \approx \frac{-\Delta CBV}{1-CBV_{rest}} \approx -\Delta CBV. \quad \text{Eq. 3}$$

Comparing Eqs. 2 and 3 makes it clear that both iron-oxide-based and VASO signal changes are linearly proportional to changes in CBV, with different normalization factors. The normalization must be kept in mind, when considering brain areas with inhomogeneous CBV_{rest} distributions, such as the different cortical layers in layer-dependent fMRI analysis (Goense et al., 2007; Weber et al., 2008). When the baseline CBV distribution across cortical laminae is known, iron-oxide signal changes can be used to estimate absolute CBV changes in units of ml per tissue in addition to the relative CBV change in units of percent (Kim and Kim, 2011).

2.4. Measurement Parameters

MRI data acquisitions were conducted in six healthy participants (3 females, age 24-32 years). All procedures were approved by the Ethics Committee of the University of Leipzig. Informed

written consent was given by all volunteers. SS-SI-VASO was implemented on a MAGNETOM 7 T scanner (Siemens Healthcare, Erlangen, Germany) equipped with an SC72 gradient coil (Siemens Healthcare). For radiofrequency (RF) transmission and reception, a single-channel-transmit/24-channel-receive head coil (Nova Medical, Wilmington, MA, USA) was used. The positioning of the functional slices and flip-angle adjustment were based on previously acquired whole-brain MP2RAGE T_1 maps (Marques et al., 2010) and MAFI B_1 maps (Boulant et al., 2009). The image acquisition and evaluation pipeline are summarized in Fig. 1. Functional BOLD and VASO data were acquired in five axial slices aligned perpendicular to the participant's M1 area, using a two-dimensional single-shot echo planar imaging (EPI) readout. Sequence parameters were: TE/TI1/TI2/TR = 18/1000/2500/3000 ms, excitation flip angle α = 130° (see discussion), partial Fourier factor = 5/8, and a corresponding vendor-provided homodyne online image reconstruction algorithm was used. In order to obtain a blood nulling time at TI1 = 1000 ms, which is approximately 200 ms lower than the estimated arterial arrival time in the sensorimotor cortex (Mildner et al., 2014), the inversion efficiency was adjusted to be equal to 85%. This corresponds to a sensitivity decrease of approximately 31%. The blood nulling time is calculated based on the assumed value of blood T_1 = 2100 ms (Zhang et al., 2012), following earlier VASO studies at 7 T (Huber et al., 2014a; Huber et al., 2014b). Nominal in-plane resolution was 0.78 x 0.78 mm^2. Since human M1 cortex has a thickness of approximately 4 mm (Fischl and Dale, 2000), up to 5 voxels are evaluated for the layer-dependency. The imaging matrix was 64 x 64 and the FOV was 50 mm. Effective gradient parameters used during EPI were: strength = 40 mT/m; slew rate = 198 T/m/s. In all participants, k-space acquisition took less than 40 ms with a bandwidth of 1132 Hz/pixel in read direction. Based on simulations assuming a tissue T_2* of 28 ms (Koopmans et al., 2008; Pfeuffer et al., 2004), the corresponding T_2* blurring and PSF broadening results in a signal leakage of 14% from one voxel into the neighboring voxels along the phase-encoding direction. This blurring is not corrected for and results in slightly coarser resolution than the nominal voxel size. Depending on the participants' M1 curvature, the nominal EPI slice thickness set between 1.2 and 2 mm. In order to minimize aliasing artifacts, phase oversampling between 0 and 15% was used depending on the individual anatomy. In order to determine the border between GM and cerebrospinal fluid (CSF) independently of distortions, T_1 maps were calculated from additional inversion-recovery EPI acquisitions with multiple inversion times (TIs) of 36/200/300/1200/1500 ms, and with acquisition parameters otherwise identical to the functional scans.

A 12-min unilateral finger-tapping stimulation paradigm (alternating 30-s rest vs. 30-s tapping) was used to induce BOLD and VASO signal changes in the central sulcus. The tapping consisted of pinch-like motion and touch of index finger, middle finger, ring finger, and little finger (consecutively) towards and away from the thumb with a self-paced frequency of approximately 0.25 - 0.75 Hz. Two 12-min stimulation experiments were done in each participant, one with tapping of right-hand fingers and one with tapping of left-hand fingers.

2.5. Data analysis

Signals from all receive channels were reconstructed separately, and the resulting tSNR characteristics were evaluated. Channels with unstable signal or severe aliasing artifacts (between 0 and 8) were excluded from the subsequent sum-of-squares combination (see

supplementary Fig. S1 for more details). The perpendicularity of the acquired slices with respect to the cortical surface was quantified by comparing the CSF position in the central sulcus across adjacent slices. The GM and CSF border of the middle slice was projected onto the adjacent slices. All regions where the displacement of the surfaces defined by the projected border between adjacent slices was more than half of the voxel size were excluded from further analysis. This orthogonality threshold corresponds to a slice tilting of approximately 15° from its optimal perpendicular orientation. Due to incomplete blood nulling in outer slices, all signal-change analyses were done on the middle slice only.

Because M1 has more than double the thickness of the primary somatosensory cortex (S1), the slice orientation was optimized with respect to M1, and all data analyses were focused on the anterior GM bank of the central sulcus. Signal changes in S1 and the posterior side of the central sulcus were not included in the ROIs for quantitative analysis, if not stated differently. Cortical laminae were calculated based on the equi-volume approach (Waehnert et al., 2014), applied directly on EPI images, without the need for distortion correction or registration to a high-resolution anatomical dataset. The cortical surface is defined to be at the position where CSF signal approaches GM signal analogously to (Goense et al., 2007). Here, the terms 'cortical laminae' and 'layer-dependent' refer to sets of voxels defined by the equi-volume contouring method, and therefore do not directly refer to the cytoarchitectonically defined cortical layers. However, it should be mentioned that the method used provides highly realistic cortical contours (see Waehnert et al., 2014). In order to obtain robust signal changes within these cortical laminae, signals were averaged over the last 15 s of the tapping period, disregarding the transition period of the first 15 s. All MR images were motion corrected using SPM8 (Wellcome Department, University College London, UK). Statistical analysis was done using FSL FEAT (Version 5.98) (Worsley, 2001) without spatial smoothing. In order to minimize bias from the layer-dependent noise distribution, the z-score threshold in all depicted activation maps was kept well below the mean detection threshold for activity in M1. Doing so, relatively noisy voxels in upper cortical layers are not excluded from the analysis. Cortical profiles were calculated from the raw (unthresholded) data.

2.6. Parameters of the animal experiments

The VASO CBV results acquired in humans were validated by comparing them with well-established iron-oxide-based fMRI methods in animals at even higher spatial resolutions. Thus, the same SS-SI-VASO sequence as used in the human experiments was implemented in laboratories using iron-oxide-based fMRI in monkey or rat models. In order to obtain results that are comparable and in compliance with earlier studies in these laboratories, SS-SI-VASO experiments were conducted with the best-established stimulus protocols on each site, that is, whisker stimulation in rats (Kennerley et al., 2005) and visual stimulation in monkeys (Goense et al., 2010).

2.6.1. Experiments in monkeys

SS-SI-VASO, as described above, was implemented on a 7 T vertical primate scanner (Bruker Biospec 70/60v, Bruker Biospin, Ettlingen, Germany) employing the stimulation setup described in Goense et al. (2012). For further details of experimental hardware (e.g. magnet

and RF coils) and animal preparation (e.g. anesthesia) the reader is referred to (Goense et al., 2010; Logothetis et al., 1999; Pfeuffer et al., 2004). Functional experiments with BOLD signal and iron-oxide contrast agent were acquired with a nominal resolution of 0.375 x 0.5 x 2 mm^3, 8 GE-EPI acquisition segments, 15 slices, volume TR = 6 s, TE = 20/9.6 ms. Ferumoxytol (Feraheme, AMAG Pharmaceuticals, Waltham, MA, USA) was injected at a dose of 8 mg/kg. The SS-SI-VASO parameters were TE/TI1/TI2/TR = 7.8/785/2285/3000 ms and 0.633 x 0.75 x 3 mm^3 nominal voxel size. VASO images were non-linearly registered to the iron-oxide and BOLD data using the software package MIPAV (Bazin et al., 2007). fMRI response in V1 was evoked by means of a rotating ring checkerboard presentation (alternating 30-s rest vs. 30-s stimulation) (Goense et al., 2012). Experiments were approved by the local authorities (Regierungspräsidium Baden-Württemberg, Germany) and were in full compliance with the guidelines of the European Community (EUVD 86/609/EEC) for the care and use of laboratory animals.

2.6.2. Experiments in rats

SS-SI-VASO, as described above, was also implemented on a 7 T rodent scanner (Bruker BioSpec, 70/30, Bruker Biospin) as reported in (Kennerley et al., 2013) employing the experimental setup described in (Kennerley et al., 2012a). In order to account for the faster blood flow in rats as compared with primates (Calamante et al., 1999), a global adiabatic 90° spin-reset pulse was played out before every TR, to control the steady-state of the entire magnetization within the transmit coil (Lu, 2008). The amplitude and phase shape functions of this pulse were adapted from the TR-FOCI pulse class, designed for use at 7 T (Hurley et al., 2010). In order to convert this pulse from an inversion pulse to a 90° saturation pulse, a 90° phase skip of the pulse amplitude was introduced halfway through the pulse duration, resulting in an inversion efficiency of 50%. The TR time was set at 3200 ms, and a BOLD image was acquired 1100 ms after global saturation. The inversion pulse was applied 400 ms thereafter, and the VASO image was acquired at the blood nulling time 1030 ms after the inversion. TE was equal to 13.1 ms, while the nominal voxel size was 0.46 x 0.46 x 3 mm^3. The functional response in S1 was induced by electrically stimulating the left whisker pad (alternating 86-s rest vs. 16-s stimulation) (Kennerley et al., 2005). Experiments with iron-oxide contrast agent (MION with dose of 9 mg/kg) were conducted with the same EPI acquisition parameters. All aspects of these methods and their development were performed with UK Home Office approval under the animals (Scientific Procedures) act 1986.

3. Results

Statistical maps of the BOLD and VASO signal changes for all human subjects are shown in Fig. 2. The corresponding cortical profiles are shown in Fig. 3. We detected a robust negative VASO signal change (indicating CBV increase) across participants and across the ROIs. VASO z-scores are approximately 70% of those of the BOLD signal. This shows that a physiologically meaningful quantity, such as ΔCBV, can be measured noninvasively with VASO in humans at a laminar level with sensitivity comparable to that of GE-BOLD. Average relative signal changes across all cortical laminae and participants in M1 are (4.3 ± 0.7)% for BOLD contrast and (2.3 ± 0.5) ml/100ml for VASO, respectively.

3.1. Intracortical signal distribution

Figures 2 and 3 show highest BOLD activity at or outside the cortical surface, decreasing with cortical depth as expected (De Martino et al., 2013; Goense et al., 2012; Kim et al., 2013; Polimeni et al., 2010). VASO signal change, on the other hand, has its peak 1 - 2 voxels (0.8 - 1.6 mm) deeper within GM. This position corresponds to the upper or middle cortical lamina. This difference between VASO and BOLD signal was obtained robustly across all participants (Fig. 2). Within GM, VASO signal change tends to decrease in deeper layers similar to BOLD.

3.2. Time courses

The normalized time courses shown in Fig. 4 suggest relatively small lamina-dependent differences in response dynamics compared to the absolute signal-change magnitude. In the BOLD signal time-courses at the cortical surface, a trend towards a stronger overshoot after task onset is seen, and a stronger undershoot after task offset. The time course during the post-stimulus undershoot is significantly different for surface laminae compared to deeper cortical laminae ($p < 0.05$ after multiple-comparison correction across time steps), but the time course differences do not reach statistical significance during the overshoot period. The feature of stronger overshoot in superficial compared to deeper laminae is more pronounced, however, in VASO time courses. In the period between 12 s and 21 s after task onset, upper cortical laminae show significantly greater relative signal change compared to the deeper cortical laminae ($p < 0.05$ after multiple-comparison correction across time steps).

3.3. Functional response in the ipsilateral hemisphere

Imaging the left central sulcus during a left-hand finger-tapping task yielded statistically significant signal changes. M1 shows a positive BOLD signal change and CBV increase, while ipsilateral S1 shows a negative BOLD and CBV decrease in all participants (Fig. 5). Average signal changes of ipsilateral BOLD and VASO responses were (1.4 ± 0.5)% and (0.75 ± 0.2) ml/100ml respectively in M1 and (−0.7 ± 0.3)% and (−0.3 ± 0.1) ml/100ml in S1, respectively. The mean negative responses in S1 are not only smaller in amplitude than in M1, but also in spatial extent. This means that the signal response averaged over a combined ROI across S1 would show a positive overall response ((0.19 ± 0.11) ml/100 ml for VASO and (0.15 ± 0.16)% for BOLD), as seen in earlier studies using coarser resolution or after spatial smoothing, where activated voxels contain signal from both sides of the sulcus (Dettmers et al., 1995; Shibuya et al., 2014). Low noise in the profiles and time courses and minimal point-to-point scatter is shown in Fig. 5b (cortical profiles) and Fig. 5c (time courses). This indicates that the relatively small ipsilateral responses are highly robust, and implies that the averaged data are not noise-dominated.

3.4. Validation with animal results

The cortical profiles of BOLD and VASO signal change in rat S1 and monkey M1 are highly consistent across the species (Fig. 6) and are also very similar to humans (Fig. 3). In all species, BOLD signal is highest at the cortical surface and has a variably pronounced ‘shoulder’ in the middle cortical laminae (Fig. 3 and Fig. 5). VASO signal change peaks below the cortical surface across species and brain regions with comparable signal changes in the upper and middle

laminae. The corresponding values of Δ*CBV* [ml/100ml] recorded with VASO in upper / middle laminae are 2.6 ± 0.4 / 2.2 ± 0.4 in human M1; 2.3 ± 0.3 / 2.0 ± 0.2 in monkey V1; and 1.2 ± 0.2 / 1.1 ± 0.2 in rat S1. Cortical profiles of iron-oxide-based fMRI are comparable with VASO signal profiles, but with small differences at the cortical surface, where VASO shows a trend towards higher relative signal changes compared to those obtained with iron oxide. VASO and iron-oxide-based fMRI have conceptually different contrast mechanisms, resulting in different normalization of their CBV weightings (Eqs. 2 and 3). Hence, the baseline distribution of CBV_{rest} needs to be taken into account when comparing and interpreting differences between the two contrasts. Using Eq. 1, CBV_{rest} can be estimated (Fig. 7a-c) and used to convert the cortical profiles of normalized relative CBV change in units of CBV_{rest} (Fig. 7d) to cortical profiles of absolute blood volume change in units of ml/100ml.

Cortical profiles of iron-oxide CBV change in units of %, which are shown in Fig. 7e, are highly consistent with the results from previous studies in the respective animals (Goense et al., 2012; Goense et al., 2007; Kennerley et al., 2009; Kennerley et al., 2005).

4. Discussion

It has been claimed that noninvasive CBV-based fMRI could be used to map local changes of neural activity in human brain with better specificity than GE-BOLD (Kennerley et al., 2005; Zhao et al., 2006). Previous low-resolution applications of VASO have suggested that the signal is more confined to GM than the GE-BOLD signal, which is known to peak in voxels at the cortical surface (Huber et al., 2014a; Huber et al., 2014b). In the current study, these insights are taken one step further with sub-millimeter resolution fMRI, allowing high resolution layer-dependent analysis. The results presented here confirm that the VASO signal change is less dominated by the surface vasculature compared to GE-BOLD signal, and represents functional tissue responses with less contamination by the macrovasculature. The SNR limitations of sub-millimeter non-BOLD fMRI in humans, which have, so far, hampered high-resolution comparisons of CBV and BOLD signal in humans, can be overcome with the intrinsically high CNR of SS-SI-VASO.

The slower VASO signal change in deeper cortical laminae and the stronger overshoot in superficial laminae are consistent with previous laminar-dependent results from studies with iron oxides in cat V1 (Jin and Kim, 2008b; Yacoub et al., 2006). The weaker relative post-activation undershoot in deeper cortical laminae is not consistent with earlier studies in cat V1 (Jin and Kim, 2008b) and human V1 (Siero et al., 2014), which may be due to different interactions of actively and passively controlled vasculature for different stimulus durations used in those studies. The stimulus durations in the respective references were 60 s (Jin and Kim, 2008b) and 0.5 – 8 s (Siero et al., 2014) compared to 30 s in this study.

4.1. Functional response in the ipsilateral hemisphere

Figure 5 shows that finger tapping surprisingly evokes a positive response in ipsilateral M1, but a negative response in ipsilateral S1. The task response in ipsilateral M1 has been found to be highly dependent on stimulus paradigm and strength. While low-force (usually 5% of individual maximal voluntary contraction) has been shown to evoke a negative BOLD response, and reductions in blood flow and metabolism in ipsilateral sensorimotor ROIs

(Dettmers et al., 1995; Hamzei et al., 2002; Stefanovic et al., 2004), responses have been observed to become positive when stronger forces and more demanding tasks are used (Dettmers et al., 1995; Shibuya et al., 2014). Even though the corticospinal tract is predominantly a crossed pathway, which suggests contralateral M1 responses only, bilateral motor representations have been reported in several studies (Cramer et al., 1999; Dettmers et al., 1995; Donchin et al., 2002). Hence, the positive ipsilateral response during unilateral motion seen in the present study could be interpreted as part of the bilateral motor representation. This requires further investigation.

Figure 5 showed that a unilateral sensory stimulation produces a robust negative ipsilateral response in S1. This is consistent with the literature for humans (Mullinger et al., 2014; Schafer et al., 2012) and animals (Boorman et al., 2010). However, none of the above-mentioned studies of ipsilateral sensorimotor activation had a sufficient resolution to distinguish or exclude the separate contributions from S1 and M1. Thus, direct comparisons with our results (Fig. 5) could be misleading. It needs to be mentioned that partial volume effects of macrovasculature draining or feeding the opposing sides of the central sulcus can complicate layer-dependent interpretation of the results in Fig. 5. For example, pial veins within the sulcus can drain both M1 and S1, and hence their BOLD signal might reflect a mixture of activity in both areas. These types of specificity limitations of BOLD signal changes, arising from large veins in the sulcus, can make it difficult to interpret separately the corresponding BOLD signal from opposite sides of the sulcus.

The robust detection of relatively small layer-dependent ipsilateral responses with VASO during a 12-min experiment suggests its applicability in future studies, for example, those investigating the afferent-efferent characteristics of the cortex.

4.2. Uncertainties in arterial and venous blood T_1

It has been shown recently, that the arterial blood T_1 is approximately 100 – 200 ms longer than venous blood T_1 (Grgac et al., 2012; Rane and Gore, 2013). When only one value is assumed for both blood compartments, as in this study, the chosen TI can differ from the true blood nulling time by 35 – 70 ms. The corresponding incomplete blood nulling can result in an error in the VASO signal change of about 8% relative to the total VASO signal change. This means that potentially different arterial and venous blood compositions in different cortical laminae can be accompanied with small biases in the VASO signal change. In a worst case, the measured CBV change of 2.3 ± 0.5 ml/100ml in human M1 might have an additional source of uncertainty, to become 2.3 ± 0.5 (inter-subject standard deviation) ± 0.17 (uncertainty in arterial and venous blood T_1) ml/100ml. Since the uncertainty in arterial and venous blood T_1 is considerably smaller than inter-subject variation, the ensuing error is considered to be tolerable here, and has no qualitative impact in the interpretation of the cortical profiles shown.

4.3. Potential artifacts of dynamic CSF volume change

Functional changes in the partial voluming of CSF and GM could affect VASO signal and make direct interpretation of ΔCBV in VASO experiments more difficult (Donahue et al., 2006; Jin and Kim, 2010; Piechnik et al., 2009). CSF contamination in VASO could mimic VASO signal

change at the cortical surface and distort the corresponding cortical profiles (Jin and Kim, 2010). Here, the steady-state of CSF and GM magnetizations was manipulated independently of TR by increasing the nominal excitation pulse flip angle. Based on simulations of GM steady-state *z*-magnetization and CSF steady-state *z*-magnetization, a nominal flip angle of $\alpha = 130°$ was chosen. These simulations are based on assumed T_1 values of 1.9 s and 4.0 s for GM and CSF, respectively. The application of a flip angle of $\alpha = 130°$ results in an SNR penalty of 9% compared to the application of the Ernst angle. This flip angle results in a BOLD-corrected VASO image with almost no signal contrast between GM and CSF (see Fig. 1e), which is thus insensitive to any functional volume redistribution of GM and CSF. In contrast with the CSF-nulled ACDC VASO (Scouten and Constable, 2008) or VASO FLAIR (Donahue et al., 2006) techniques, the VASO signal changes in this study reflect both components of the CBV change—the CBV increase that is compensated by a GM volume decrease as well as the CBV increase that is compensated by CSF volume decrease—with the same weighting.

4.4. Comparison of VASO and iron-oxide-based fMRI in animals

VASO was applied in animals in order to validate its CBV weighting. Jin and Kim (2006; 2008a) compared the layer dependence of the VASO signal with that using an iron-oxide contrast agent. In order to minimize inflow of 'fresh' blood during the inversion time, VASO images had to be acquired 500 ms before the blood nulling time, introducing a flow weighting as with ASL-FAIR experiments lacking a control condition. In these studies, differences of relative signal change obtained with VASO and iron oxides in upper cortical layers were interpreted to arise from inflow effects and limited BOLD contamination (Jin and Kim, 2006). Further quantitative studies were needed to reveal the underlying CBV sensitivity of VASO in comparison to iron-oxide-based fMRI independent of such flow contaminations (Jin and Kim, 2008a).

Across GM regions and species, the general vascular layout of large vessels is broadly similar. For example, larger arterioles or larger venules feed or drain the cortical laminae from the surface (Duvernoy et al., 1981). The microvessels are distributed inside GM across the cortical layers. There are subtle and specific differences across cortical layers in different brain areas (Duvernoy et al., 1981). For all three stimulation tasks used here, the major part of the neutrally driven energy consumption increase is not expected to occur at the cortical surface at the site of large pial vasculature, but it is expected to occur within the cortex, distributed across the cortical layers. Much of the energy use is expected in middle cortical layers, corresponding to the thalamocortical input layer IV in V1 and S1, and in M1 increased activity in thalamocortical and corticocortical input layer V (Porter and Lemon, 1995) and in cortico-cortical input layer II/III (Yu et al., 2014). Because BOLD and VASO MRI data characterize lamina-dependent vascular changes, the exact correspondence between neural activity changes and vascular changes in individual cytoarchitecturally-defined cortical layers is still unknown. The resulting cortical profiles of BOLD and VASO signal changes are rather expected to reflect the neurally driven microvascular response in a particular cortical lamina combined with the signal response of diving arteries and veins passing through that layer. Depending on the MRI resolution, a given cortical lamina in the MRI data can contain multiple anatomically defined cortical layers of different cytoarchitecture.

4.5. Vascular origin of BOLD, VASO and iron-oxide-based fMRI

The different cortical profile shapes of BOLD, VASO, and iron-oxide-based signal depend partly on the influence of macrovascular contributions in the different modalities, so they must be discussed with respect to expected underlying vascular features.

A qualitative schematic illustration of the expected vascular contributions in the respective methodologies is shown in Fig. 8. It is shown how a certain layer-dependent response might be transformed into the detectable laminar signal change of the corresponding modalities. In order to discuss the different physiological point spread function of BOLD, VASO and iron-oxide-based fMRI, a double peak response is used here as reported earlier in rat M1 (Yu et al., 2014). This example is chosen for illustrative reasons because it clearly visualizes different macrovascular contamination in upper and deeper cortical laminae.

The GE-BOLD signal change at 7 T can be considered to be dominated by translaminar diving venules and pial veins rather than by intralaminar capillaries (Uludag et al., 2009). Hence, the majority of the BOLD signal reflects oxygenation changes in veins draining multiple layers, making it difficult to break down the signal into layer-dependent activity. The contribution of intralaminar capillary BOLD signal with layer-dependent specificity is expected to be relatively low compared to macrovascular BOLD signal (upper row in Fig. 8).

VASO fMRI is expected to capture CBV changes in small intralaminar arterioles (Tian et al., 2010), and in capillaries to some extent (Stefanovic et al., 2008), but almost no signal is expected to come from venules (Hillman et al., 2007). Additionally, VASO fMRI is expected to capture CBV changes in larger translaminar diving arterioles (Tian et al., 2010). The diameter of these diving arterioles is larger in the upper cortical laminae and becomes smaller with increasing cortical depth (Duvernoy et al., 1981). During functional activity, their relative vessel diameter increase is homogeneous across the cortical laminae (Tian et al., 2010). This suggests that the absolute CBV change of those diving arterioles is smallest in deep cortical laminae and somewhat larger in upper cortical laminae. The Δ*CBV* contribution from pial arteries, which visibly dilate in optical imaging spectroscopy studies (Kennerley et al., 2012b), are also expected to contribute to the global CBV change. This macrovascular contribution could result in the highest VASO signal change in upper cortical laminae (middle row in Fig. 8).

In contrast to VASO fMRI, the relative signal change recorded with iron oxide is inherently normalized to the local baseline blood volume. This normalization introduces severe inverse macrovascular weighting at the location of large translaminar arterial and venous vessels. Since the macrovascular baseline CBV can vary up to a factor of five across measured laminae at and below the cortical surface (see Fig. 7a or (Goense et al., 2007; Kennerley et al., 2005; Kim et al., 2013)), the intralaminar microvasculature response in upper cortical laminae appears suppressed in the resulting cortical profiles (Fig. 7d and bottom row in Fig. 8).

The large macrovascular contribution at the surface and the fact that iron-oxide-based CBV-changes are usually reported in percent change tends to underestimate the actual CBV change (ΔCBV) at the surface. Thus the widely reported feature that CBV-sensitive iron-oxide-based fMRI shows highest activity in deeper cortical layers (Kim et al., 2013) at the site of thalamocortical input layers does not necessarily suggest high local specificity, but might in fact be due to inverse macrovascular weighting in the upper cortical laminae. Furthermore, in iron-oxide-based fMRI, the high baseline CBV at the cortical surface can result in low MR signal

intensity. If SNR at the surface is limited, the corresponding layer-dependent detection threshold can be higher than the signal change at the cortical surface (Goense et al., 2012).

In summary, among the three investigated fMRI contrasts in this study, GE-BOLD contrast has the strongest relative macrovascular contamination. VASO and iron-oxide-based fMRI also have macrovascular weighting or contamination from the upper cortical laminae, but to a lesser degree than BOLD fMRI. We have shown that VASO has lower sensitivity to macrovasculature than GE-BOLD, and hence higher specificity to functionally driven changes in microvasculature. But layer-dependent cortical profiles of VASO signal clearly represent a sum of microvascular and macrovascular contributions, albeit with a relatively larger microvascular contribution.

Future quantitative models relying on the layer-dependent micro- and macrovasculature distribution might be able to extend the above qualitative considerations to a quantitative level (Gagnon et al., 2013; Markuerkiaga et al., 2014).

4.6. Other imaging modalities

Spin-echo (SE) BOLD fMRI has been suggested to have higher specificity to the microvasculature (Uludag et al., 2009) and its utility for laminar and columnar fMRI has been demonstrated in animals (Goense et al., 2012; Harel et al., 2006; Zhao et al., 2006) and in humans (Yacoub et al., 2005; Yacoub et al., 2008). However, it suffers from much lower sensitivity, especially at high resolution (Yacoub et al., 2005), which may limit the widespread application of the technique (Boyacioglu et al., 2014; Budde et al., 2014; Harmer et al., 2012).

5. Conclusion

We have shown that the SS-SI-VASO method can be used, at high field (7 T), to noninvasively and simultaneously investigate the cortical profiles of ΔCBV and BOLD signal. This allows us to capture layer-dependent CBV responses robustly in humans, information that was previously only accessible in animal research. Considering the different macrovascular contributions and normalization features in VASO and iron-oxide-based fMRI, cortical profiles of both contrasts are in good agreement. The data presented here suggest that VASO can be used to investigate layer-dependent responses with much reduced macrovascular contributions compared to GE-BOLD. VASO may thus play an important role in revealing top-down or afferent-efferent stimulus processing in the brain using layer-dependent fMRI, without the unwanted sensitivity to vascular changes in large draining veins that GE-BOLD suffers from.

6. Acknowledgements

We thank Domenica Wilfling and Elisabeth Wladimirow for radiographic assistance. We are grateful to Daniel Zaldivar, Thomas Steudel, and Deniz Ipek for assistance with the monkey experiments and to Prof. Nikos Logothetis for access to his experimental facilities. Preliminary accounts of this study have been presented at the ISMRM Brain Function Workshop in Charleston, SC, USA. The research was supported by the Max Planck Society. AK was supported by the UK Medical Research Council (#G1002194). MG was supported by the Initial

Training Network, HiMR, funded by the FP7 Marie Curie Actions of the European Commission (FP7-PEOPLE-2012-ITN-316716).

7. References

Bazin, P.L., Cuzzocreo, J.L., Yassa, M.A., Gandler, W., McAuliffe, M.J., Bassett, S.S., Pham, D.L., 2007. Volumetric neuroimage analysis extensions for the MIPAV software package. J Neurosci Methods 165, 111-121.

Boorman, L., Kennerley, A.J., Johnston, D., Jones, M., Zheng, Y., Redgrave, P., Berwick, J., 2010. Negative blood oxygen level dependence in the rat: a model for investigating the role of suppression in neurovascular coupling. J Neurosci 30, 4285-4294.

Boulant, N., Mangin, J.F., Amadon, A., 2009. Counteracting radio frequency inhomogeneity in the human brain at 7 Tesla using strongly modulating pulses. Magn Reson Med 61, 1165-1172.

Boyacioglu, R., Schulz, J., Muller, N.C., Koopmans, P.J., Barth, M., Norris, D.G., 2014. Whole brain, high resolution multiband spin-echo EPI fMRI at 7T: A comparison with gradient-echo EPI using a color-word Stroop task. Neuroimage 97, 142-150.

Budde, J., Shajan, G., Zaitsev, M., Scheffler, K., Pohmann, R., 2014. Functional MRI in human subjects with gradient-echo and spin-echo EPI at 9.4 T. Magn Reson Med 71, 209-218.

Calamante, F., Thomas, D.L., Pell, G.S., Wiersma, J., Turner, R., 1999. Measuring cerebral blood flow using magnetic resonance imaging techniques. J Cereb Blood Flow Metab 19, 701-735.

Cramer, S.C., Finklestein, S.P., Schaechter, J.D., Bush, G., Rosen, B.R., 1999. Activation of distinct motor cortex regions during ipsilateral and contralateral finger movements. J Neurophysiol 81, 383-387.

De Martino, F., Zimmermann, J., Muckli, L., Ugurbil, K., Yacoub, E., Goebel, R., 2013. Cortical depth dependent functional responses in humans at 7T: improved specificity with 3D GRASE. PLoS One 8, e60514.

Dettmers, C., Fink, G.R., Lemon, R.N., Stephan, K.M., Passingham, R.E., Silbersweig, D., Holmes, A., Ridding, M.C., Brooks, D.J., Frackowiak, R.S., 1995. Relation between cerebral activity and force in the motor areas of the human brain. J Neurophysiol 74, 802-815.

Donahue, M.J., Lu, H., Jones, C.K., Edden, R.A., Pekar, J.J., van Zijl, P.C., 2006. Theoretical and experimental investigation of the VASO contrast mechanism. Magn Reson Med 56, 1261-1273.

Donchin, O., Gribova, A., Steinberg, O., Mitz, A.R., Bergman, H., Vaadia, E., 2002. Single-unit activity related to bimanual arm movements in the primary and supplementary motor cortices. J Neurophysiol 88, 3498-3517.

Duvernoy, H.M., Delon, S., Vannson, J.L., 1981. Cortical blood vessels of the human brain. Brain Res Bull 7, 519-579.

Fischl, B., Dale, A.M., 2000. Measuring the thickness of the human cerebral cortex from magnetic resonance images. Proc Natl Acad Sci USA 97, 11050-11055.

Gagnon, L., Sakadzic, S., Devor, A., Fang, Q., Lesage, F., Mandeville, E.T., Srinivasan, V.J., Yaseen, M.A., Roussakis, E., Lo, E.H., Vinogradov, S., Buxton, R.B., Dale, A.M., Boas, D.A., 2013. Modeling the fMRI signals at the microscopic level using quantitative optical microscopy measurements. In Proceedings of the 21st Meeting of ISMRM, Salt Lake City, UT, USA, p. 3244.

Goense, J., Merkle, H., Logothetis, N.K., 2012. High-resolution fMRI reveals laminar differences in neurovascular coupling between positive and negative BOLD responses. Neuron 76, 629-639.

Goense, J., Logothetis, N.K., Merkle, H., 2010. Flexible, phase-matched, linear receive arrays for high-field MRI in monkeys. Magn Reson Imaging 28, 1183-1191.

Goense, J.B., Zappe, A.C., Logothetis, N.K., 2007. High-resolution fMRI of macaque V1. Magn Reson Imaging 25, 740-747.

Grgac, K., van Zijl, P.C., Qin, Q., 2012. Hematocrit and oxygenation dependence of blood (1) H(2) O T(1) at 7 tesla. Magn Reson Med 70, 1153-1159.

Hamzei, F., Dettmers, C., Rzanny, R., Liepert, J., Buchel, C., Weiller, C., 2002. Reduction of excitability ("inhibition") in the ipsilateral primary motor cortex is mirrored by fMRI signal decreases. Neuroimage 17, 490-496.
Harel, N., Lin, J., Moeller, S., Ugurbil, K., Yacoub, E., 2006. Combined imaging-histological study of cortical laminar specificity of fMRI signals. Neuroimage 29, 879-887.
Harmer, J., Sanchez-Panchuelo, R.M., Bowtell, R., Francis, S.T., 2012. Spatial location and strength of BOLD activation in high-spatial-resolution fMRI of the motor cortex: a comparison of spin echo and gradient echo fMRI at 7 T. NMR Biomed 25, 717-725.
Hetzer, S., Mildner, T., Moller, H.E., 2011. A modified EPI sequence for high-resolution imaging at ultra-short echo time. Magn Reson Med 65, 165-175.
Hillman, E.M.C., Devor, A., Bouchard, M.B., Dunn, A.K., Krauss, G.W., Skoch, J., Bacskai, B.J., Dale, A.M., Boas, D.A., 2007. Depth-resolved optical imaging and microscopy of vascular compartment dynamics during somatosensory stimulation. Neuroimage 35, 89-104.
Hua, J., Jones, C.K., Qin, Q., van Zijl, P.C., 2013. Implementation of vascular-space-occupancy MRI at 7T. Magn Reson Med 69, 1003-1013.
Huber, L., Ivanov, D., Krieger, S.N., Streicher, M.N., Mildner, T., Poser, B.A., Moller, H.E., Turner, R., 2014a. Slab-selective, BOLD-corrected VASO at 7 tesla provides measures of cerebral blood volume reactivity with high signal-to-noise ratio. Magn Reson Med 72, 137-148.
Huber, L., Goense, J., Kennerley, A.J., Ivanov, D., Krieger, S.N., Lepsien, J., Trampel, R., Turner, R., Moller, H.E., 2014b. Investigation of the neurovascular coupling in positive and negative BOLD responses in human brain at 7T. Neuroimage 97, 349-362.
Hurley, A.C., Al-Radaideh, A., Bai, L., Aickelin, U., Coxon, R., Glover, P., Gowland, P.A., 2010. Tailored RF Pulse for Magnetization Inversion at Ultrahigh Field. Magn. Reson. Med. 63, 51-58.
Jin, T., Kim, S.G., 2006. Spatial dependence of CBV-fMRI: a comparison between VASO and contrast agent based methods. In Proceedings of the 28th IEEE EMBS Annual International Conference, New York, NY, USA, pp. 1, 25-28.
Jin, T., Kim, S.-G., 2008a. Improved cortical-layer specificity of vascular space occupancy fMRI with slab inversion relative to spin-echo BOLD at 9.4 T Neuroimage 40, 59-67.
Jin, T., Kim, S.G., 2008b. Cortical layer-dependent dynamic blood oxygenation, cerebral blood flow and cerebral blood volume responses during visual stimulation. Neuroimage 43, 1-9.
Jin, T., Kim, S.G., 2010. Change of the cerebrospinal fluid volume during brain activation investigated by T(1rho)-weighted fMRI. Neuroimage 51, 1378-1383.
Kemper, V.G., De Martino, F., Vu, A.T., Poser, B.A., Feinberg, D.A., Yacoub, E., Goebel, R., 2014. Evaluation of point spread function and functional sensitivity of 3D-GRASE and 2D spin-echo EPI for sub-millimeter- resolution fMRI at 7 T. In Proceedings of the 22nd Annual Meeting of ISMRM, Milan, Italy, p. 2987.
Kennerley, A.J., Berwick, J., Martindale, J., Johnston, D., Zheng, Y., Mayhew, J.E., 2009. Refinement of optical imaging spectroscopy algorithms using concurrent BOLD and CBV fMRI. Neuroimage 47, 1608-1619.
Kennerley, A.J., Mayhew, J.E., Boorman, L., Zheng, Y., Berwick, J., 2012a. Is optical imaging spectroscopy a viable measurement technique for the investigation of the negative BOLD phenomenon? A concurrent optical imaging spectroscopy and fMRI study at high field (7 T). Neuroimage 61, 10-20.
Kennerley, A.J., Harris, S., Bruyns-Haylett, M., Boorman, L., Zheng, Y., Jones, M., Berwick, J., 2012b. Early and late stimulus-evoked cortical hemodynamic responses provide insight into the neurogenic nature of neurovascular coupling. J Cereb Blood Flow Metab 32, 468-480.
Kennerley, A.J., Berwick, J., Martindale, J., Johnston, D., Papadakis, N., Mayhew, J.E., 2005. Concurrent fMRI and optical measures for the investigation of the hemodynamic response function. Magn. Reson. Med. 54, 354-365.
Kennerley, A.J., Huber, L., Mildner, T., Mayhew, J.E., Turner, R., Möller, H.E., Berwick, J., 2013. Does VASO contrast really allow measurement of CBV at High Field (≥7T)? An in-vivo quantification using

concurrent Optical Imaging Spectroscopy. In Proceedings of the 21st Meeting of ISMRM, Salt Lake City, UT, USA, p. 757.
Kim, S.G., Harel, N., Jin, T., Kim, T., Lee, P., Zhao, F., 2013. Cerebral blood volume MRI with intravascular superparamagnetic iron oxide nanoparticles. NMR Biomed 26, 949-962.
Kim, T., Kim, S.G., 2011. Temporal dynamics and spatial specificity of arterial and venous blood volume changes during visual stimulation: implication for BOLD quantification. J Cereb Blood Flow Metab 31, 1211-1222.
Koopmans, P.J., Barth, M., Orzada, S., Norris, D.G., 2011. Multi-echo fMRI of the cortical laminae in humans at 7 T. Neuroimage 56, 1276-1285.
Koopmans, P.J., Manniesing, R., Niessen, W.J., Viergever, M.A., Barth, M., 2008. MR venography of the human brain using susceptibility weighted imaging at very high field strength. Magn Reson Mater Phy 21, 149-158.
Koopmans, P.J., Barth, M., Norris, D.G., 2010. Layer-specific BOLD activation in human V1. Hum Brain Mapp 31, 1297-1304.
Logothetis, N.K., Guggenberger, H., Peled, S., Pauls, J., 1999. Functional imaging of the monkey brain. Nat Neurosci 2, 555-562.
Lu, H., Hua, J., van Zijl, P.C., 2013. Noninvasive functional imaging of cerebral blood volume with vascular-space-occupancy (VASO) MRI. NMR Biomed 26, 932-948.
Lu, H., 2008. Magnetization `reset' for non-steady-state blood spins in Vascular-Space-Occupancy (VASO) fMRI. In Proceedings of the 16th Annual Meeting of ISMRM, Toronto, ON, Canada, p. 406.
Mandeville, J.B., 2012. IRON fMRI measurements of CBV and implications for BOLD signal. Neuroimage 62, 1000-1008.
Markuerkiaga, I., Barth, M., Norris, D.G., 2014. Towards a vascular model of layer specific activation., In Proceedings of the 22nd Annual Meeting of ISMRM, Milan, Italy, p. 3093.
Marques, J.P., Kober, T., Krueger, G., van der Zwaag, W., Van de Moortele, P.F., Gruetter, R., 2010. MP2RAGE, a self bias-field corrected sequence for improved segmentation and T1-mapping at high field. Neuroimage 49, 1271-1281.
Mildner, T., Muller, K., Hetzer, S., Trampel, R., Driesel, W., Moller, H.E., 2014. Mapping of arterial transit time by intravascular signal selection. NMR Biomed 27, 594-609.
Mullinger, K.J., Mayhew, S.D., Bagshaw, A.P., Bowtell, R., Francis, S.T., 2014. Evidence that the negative BOLD response is neuronal in origin: a simultaneous EEG-BOLD-CBF study in humans. Neuroimage 94, 263-274.
Pfeuffer, J., Merkle, H., Beyerlein, M., Steudel, T., Logothetis, N.K., 2004. Anatomical and functional MR imaging in the macaque monkey using a vertical large-bore 7 Tesla setup. Magn Reson Imaging 22, 1343-1359.
Piechnik, S.K., Evans, J., Bary, L.H., Wise, R.G., Jezzard, P., 2009. Functional Changes in CSF Volume Estimated Using Measurement of Water T2 Relaxation. Magn. Reson. Imaging 61, 579-586.
Polimeni, J.R., Fischl, B., Greve, D.N., Wald, L.L., 2010. Laminar analysis of 7T BOLD using an imposed spatial activation pattern in human V1. Neuroimage 52, 1334-1346.
Porter, R., Lemon, R.N., 1995. Corticospinal Function and Voluntary Movement. Oxford University Press, Oxford, UK.
Rane, S.D., Gore, J.C., 2013. Measurement of T1 of human arterial and venous blood at 7T. Magn Reson Imaging 31, 477-479.
Ress, D., Glover, G.H., Liu, J., Wandell, B., 2007. Laminar profiles of functional activity in the human brain. Neuroimage 34, 74-84.
Schafer, K., Blankenburg, F., Kupers, R., Gruner, J.M., Law, I., Lauritzen, M., Larsson, H.B., 2012. Negative BOLD signal changes in ipsilateral primary somatosensory cortex are associated with perfusion decreases and behavioral evidence for functional inhibition. Neuroimage 59, 3119-3127.
Scouten, A., Constable, R.T., 2008. VASO-based calculations of CBV change: Accounting for the dynamic CSF volume. Magn. Reson. Med. 58, 308-315.

Shibuya, K., Kuboyama, N., Tanaka, J., 2014. Changes in ipsilateral motor cortex activity during a unilateral isometric finger task are dependent on the muscle contraction force. Physiol Meas 35, 417-428.
Siero, J.C., Hendrikse, J., Hoogduin, H., Petridou, N., Luijten, P., Donahue, M.J., 2014. Cortical depth dependence of the BOLD initial dip and poststimulus undershoot in human visual cortex at 7 Tesla. Magn Reson Med, DOI: 10.1002/mrm.25349.
Siero, J.C., Petridou, N., Hoogduin, H., Luijten, P.R., Ramsey, N.F., 2011. Cortical depth-dependent temporal dynamics of the BOLD response in the human brain. J Cereb Blood Flow Metab 31, 1999-2008.
Stefanovic, B., Warnking, J.M., Pike, G.B., 2004. Hemodynamic and metabolic responses to neuronal inhibition. Neuroimage 22, 771-778.
Stefanovic, B., Hutchinson, E., Yakovleva, V., Schram, V., Russell, J.T., Belluscio, L., Koretsky, A.P., Silva, A.C., 2008. Functional reactivity of cerebral capillaries. J Cereb Blood Flow Metab 28, 961-972.
Tian, P., Teng, I.C., May, L.D., Kurz, R., Lu, K., Scadeng, M., Hillman, E.M., De Crespigny, A.J., D'Arceuil, H.E., Mandeville, J.B., Marota, J.J., Rosen, B.R., Liu, T.T., Boas, D.A., Buxton, R.B., Dale, A.M., Devor, A., 2010. Cortical depth-specific microvascular dilation underlies laminar differences in blood oxygenation level-dependent functional MRI signal. Proc Natl Acad Sci USA 107, 15246-15251.
Trampel, R., Bazin, P.L., Schäfer, A., Heidemann, R.M., Ivanov, D., Lohmann, G., Geyer, S., Turner, R., 2012. Laminar-specific fingerprints of different sensorimotor areas obtained during imagined and actual finger tapping. In Proceedings of the 20th Annual Meeting of ISMRM, Melbourne, Australia, p. 2775.
Triantafyllou, C., Hoge, R.D., Krueger, G., Wiggins, C.J., Potthast, A., Wiggins, G.C., Wald, L.L., 2005. Comparison of physiological noise at 1.5 T, 3 T and 7 T and optimization of fMRI acquisition parameters. Neuroimage 26, 243-250.
Tropres, I., Grimault, S., Vaeth, A., Grillon, E., Julien, C., Payen, J.F., Lamalle, L., Decorps, M., 2001. Vessel size imaging. Magn Reson Med 45, 397-408.
Turner, R., 2002. How much cortex can a vein drain? Downstrean milustion of activation-related cerebral blood oxygenation changes. Neuroimage 16, 1062-1067.
Uludag, K., Muller-Bierl, B., Ugurbil, K., 2009. An integrative model for neuronal activity-induced signal changes for gradient and spin echo functional imaging. Neuroimage 48, 150-165.
Waehnert, M.D., Dinse, J., Weiss, M., Streicher, M.N., Waehnert, P., Geyer, S., Turner, R., Bazin, P.L., 2014. Anatomically motivated modeling of cortical laminae. Neuroimage 93 Pt 2, 210-220.
Weber, B., Keller, A.L., Reichold, J., Logothetis, N.K., 2008. The microvascular system of the striate and extrastriate visual cortex of the macaque. Cerebral Cortex 18, 2318-2330.
Worsley, K.J., 2001. Statistical analysis of activation images. In P. Jezzard, P. M. Matthews, S. M. Smith (eds). Functional MRI: An introduction to Methods. Oxford University Press, Oxford, UK, pp. 251.
Yacoub, E., Ugurbil, K., Harel, N., 2006. The spatial dependence of the poststimulus undershoot as revealed by high-resolution BOLD- and CBV-weighted fMRI. J Cereb Blood Flow Metab 26, 634-644.
Yacoub, E., Van De Moortele, P.F., Shmuel, A., Ugurbil, K., 2005. Signal and noise characteristics of Hahn SE and GE BOLD fMRI at 7 T in humans. Neuroimage 24, 738-750.
Yacoub, E., Harel, N., Ugurbil, K., 2008. High-field fMRI unveils orientation columns in humans. Proc Natl Acad Sci U S A 105, 10607-10612.
Yu, X., Qian, C., Chen, D.Y., Dodd, S.J., Koretsky, A.P., 2014. Deciphering laminar-specific neural inputs with line-scanning fMRI. Nat Methods 11, 55-58.
Zhang, X., Petersen, E.T., Ghariq, E., De Vis, J.B., Webb, A.G., Teeuwisse, W.M., Hendrikse, J., van Osch, M.J., 2012. In vivo blood T(1) measurements at 1.5 T, 3 T, and 7 T. Magn Reson Med.
Zhao, F., Wang, P., Hendrich, K., Ugurbil, K., Kim, S.G., 2006. Cortical layer-dependent BOLD and CBV responses measured by spin-echo and gradient-echo fMRI: insights into hemodynamic regulation. Neuroimage 30, 1149-1160.

Figure captions:

Fig. 1: Acquisition and evaluation procedure to obtain layer-dependent VASO and BOLD signal changes. EPI slice orientation is planned on previously acquired anatomical T_1-maps to position the imaging slices perpendicular to the cortical surface of the motor cortex **(a)**. Orthogonality is verified by projecting the cortical surfaces onto adjacent slices **(b)**. Cortical laminae are calculated from IR-EPI T_1-maps in the regions where the slices are perpendicular to the cortex **(c)**. Interleaved acquisition of VASO and BOLD time series during a finger-tapping task **(d,e)** are motion corrected and evaluated to obtain statistical activation maps of BOLD signal change and BOLD-corrected VASO signal change **(f)**.

Fig. 2: Statistical activation maps of BOLD and VASO signal change for all six participants. Z-scores of BOLD and VASO activations on the contralateral side are depicted in the GM ROIs of M1. For easy visualization of the cortical surfaces, manually drawn green lines are overlaid onto the maps in the three bottom rows of the figure. These green lines are drawn to stress the different signal origin of VASO and BOLD signal and do not necessarily indicate to the GM-CSF border. Across all participants, highest BOLD signal is seen above the cortical surface. Inside GM, the BOLD signal decreases with cortical depth. VASO signal activity, on the other hand, peaks inside GM and below the green reference line. Inside GM, VASO signal decreases with cortical depth similar to BOLD. Indications of increased functional activity in deeper cortical laminae are visible in some cases (black arrows). The reference image used as a background corresponds to the tSNR map of the EPI fMRI time series. Nominal in-plane resolution is 0.78 x 0.78 mm^2 and slice thickness is 1.2 -2 mm.

Fig. 3: Averaged cortical profiles of BOLD and VASO in human M1. BOLD signal change peaks at or above the cortical surface, while VASO peaks slightly deeper and inside GM. The point of zero cortical depth is defined as the border between GM and CSF. With the resolutions used in this study, this borderline is usually not distinguishable from the voxels with maximal CSF partial voluming. The *x*-axis refers to cortical depth in volume units normalized to cortical thickness and in units of mm, respectively. Since the GM-WM border is not very pronounced in M1, cortical thickness is taken from the literature assumed to be 4 mm (Fischl and Dale, 2000) in all participants. The approximate position of GM is schematically depicted with the shaded gray rectangle in the background.

Fig. 4: Layer-dependent VASO and BOLD signal time courses. Time courses for BOLD **(a)** and VASO **(b)** signal at different cortical depths. Compared to the amplitude of the total signal change, the differences in time courses for different cortical depths are relatively small. There is a tendency of stronger BOLD signal overshoot and undershoot at the cortical surface. An overshoot approximately 10 s after stimulus onset is also clearly visible in VASO, while the post-stimulus signal does not show a clear laminar signature. Cortical-depth-dependent differences in signal time courses could potentially reflect: local differences in neural activity, different neuro-vascular coupling, or different macrovascular contributions for different cortical laminae. For the sake of clarity, only three time courses are depicted corresponding to: cortical surface, middle cortical laminae, and deep cortical laminae. The respective ROIs are depicted in panel **c)** for a representative subject.

Fig. 5: Responses in ipsilateral M1 and S1. a) Statistical activation maps of BOLD and VASO showing the ipsilateral responses, i.e., left M1 and S1 for tapping with the left hand. M1 showed positive BOLD signal and CBV increase, while S1 showed negative BOLD and CBV decrease in all participants. *Z*-scores are overlaid on tSNR maps of the fMRI EPI-time series. **b)** Cortical profiles of BOLD and VASO signal change in S1. On both sides of the central sulcus, VASO signal change peaks in deeper cortical laminae compared to BOLD. Despite presumable partial voluming of positive and negative responses in the CSF region of the central sulcus, BOLD signal change shows a sharp signal jump. **c)** Mean time courses of BOLD and VASO signal in ROIs of M1 and S1 during right hand finger tapping and left hand finger tapping. In order to avoid partial voluming between M1 and S1, the signal from the upper laminae is excluded.

Fig. 6: Cortical profiles of relative BOLD, VASO, and iron-oxide-based signal change in animals. a) and **c)** depict cortical profiles of relative signal changes of BOLD, VASO, iron-oxide-based fMRI signal in monkey V1

and rat S1. BOLD and VASO signal distribution across the cortex is remarkably similar to human results (Fig. 3); BOLD signal peaks at or above the cortical surface with a more or less pronounced 'shoulder' in middle cortical laminae, while VASO shows a double peak distribution across species. Cortical profiles of VASO and iron-oxide-based functional responses are the same within the error of the measurements. However, a trend of higher VASO signal change close to the cortical surface can be noticed. For best comparison of the different contrasts, cortical profiles are scaled to the signal change in deeper cortical layers. The values of the unscaled signals are given in the main text. **b)** Monkey V1 (sagittal slice), **d)** rat S1 (coronal slice), statistical z-score activation maps of BOLD, VASO, and iron-oxide-based signal corresponding to cortical profiles depicted in **a)** and **c)** overlaid on the raw EPI images. The *x*-axis refers to cortical depth in volume units normalized to cortical thickness and in units of mm, respectively. Cortical profiles of ultra-high resolution FLASH signal can be used to reveal the approximate position of the cortical surface (peak) and layer IV (dip).

Fig. 7: Comparison of VASO and iron-oxide-based fMRI. Due to the inherently different normalization of VASO and iron-oxide-based fMRI (Eq. 2 and Eq. 3), layer-dependent baseline CBV_{rest} distribution must be considered. **a)**, **b)**, **c)** In monkey V1 and rat S1, CBV_{rest} is highest at the cortical surface. In rat S1, CBV_{rest} decreases continuously with cortical depth, while in monkey V1, CBV_{rest} is more homogeneous in deeper laminae, and layer IV is visible. **d)** Cortical profiles of normalized iron-oxide-based signal change ($\Delta CBV/CBV_{rest}$) of monkey V1 and rat S1 as in Fig. 5b and Fig. 5c. **e)** Cortical profiles of CBV change in units of volume change (not in units of baseline CBV) in rat S1, monkey V1 and human M1 acquired with multiple contrasts. Iron-oxide-based results without normalization are obtained by the multiplication of profiles in panels **a)** and **d)**. VASO results do not have the inherent CBV_{rest}-normalization of the iron-oxide-based fMRI so the depicted profiles directly correspond to relative signal change as given in Figs. 5a, 5b, and 5c. The profiles are strikingly similar across imaging modalities and even species and brain regions and residual differences are not significant with respect to the inter-subject variation. For best comparison of the different species and contrasts, cortical profiles are scaled to the signal change in deeper cortical layers. The values of the unscaled CBV changes are given in the main text.

Fig. 8: Schematic illustration of the investigated fMRI signals and their sensitivity to micro- and macro-vasculature. All three contrasts, BOLD signal, VASO and iron-oxide-based fMRI are sensitive to both changes in microvasculature and changes in macrovasculature, but with different weightings. The black dashed regions refer to macrovasculature spreading across cortical layers, and microvasculature confined to individual cortical layers, respectively. The term ΔY refers to the changes in the blood oxygenation. The expected sensitivity is considered in an example of enhanced activity in upper and lower cortical layers. It reflects the cortico-cortical input response of rat M1 (Yu et al., 2014) for activity in M1 and is considered an illustrative example only. BOLD signal change has a large contamination from large diving veins and pial veins draining the activated layers. In VASO signal changes, the CBV change of feeding arteries supplying the activated layers introduces a weighting of macrovasculature beyond the activated laminae. In iron-oxide-based methods, the inherent normalization to total baseline CBV introduces an inverse weighting of large vessels at and below the cortical surface.

9. Figure

Click here to download 9. Figure: fig1_method.pdf

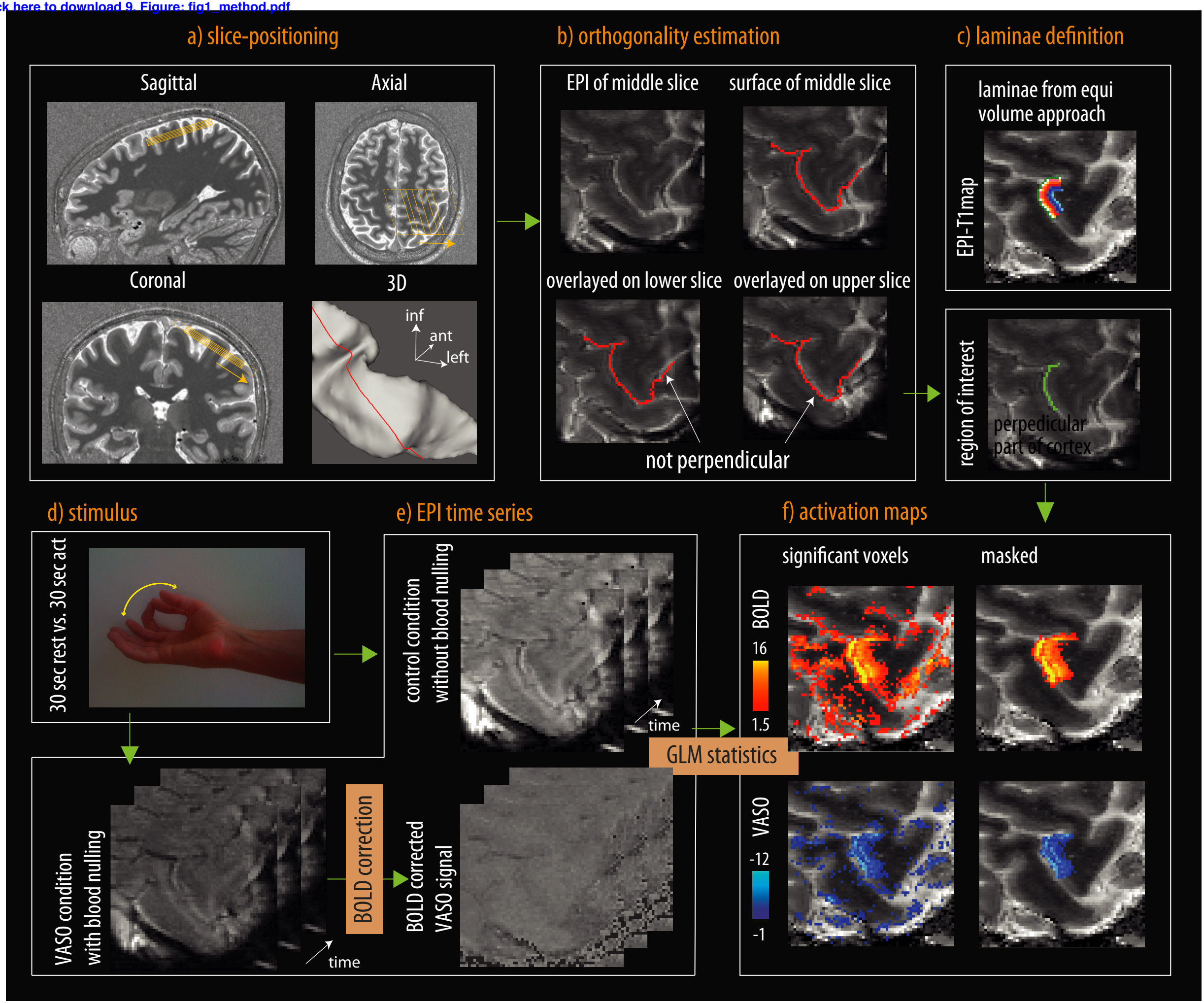

9. Figure

Click here to download 9. Figure: fig2_allmaps.pdf

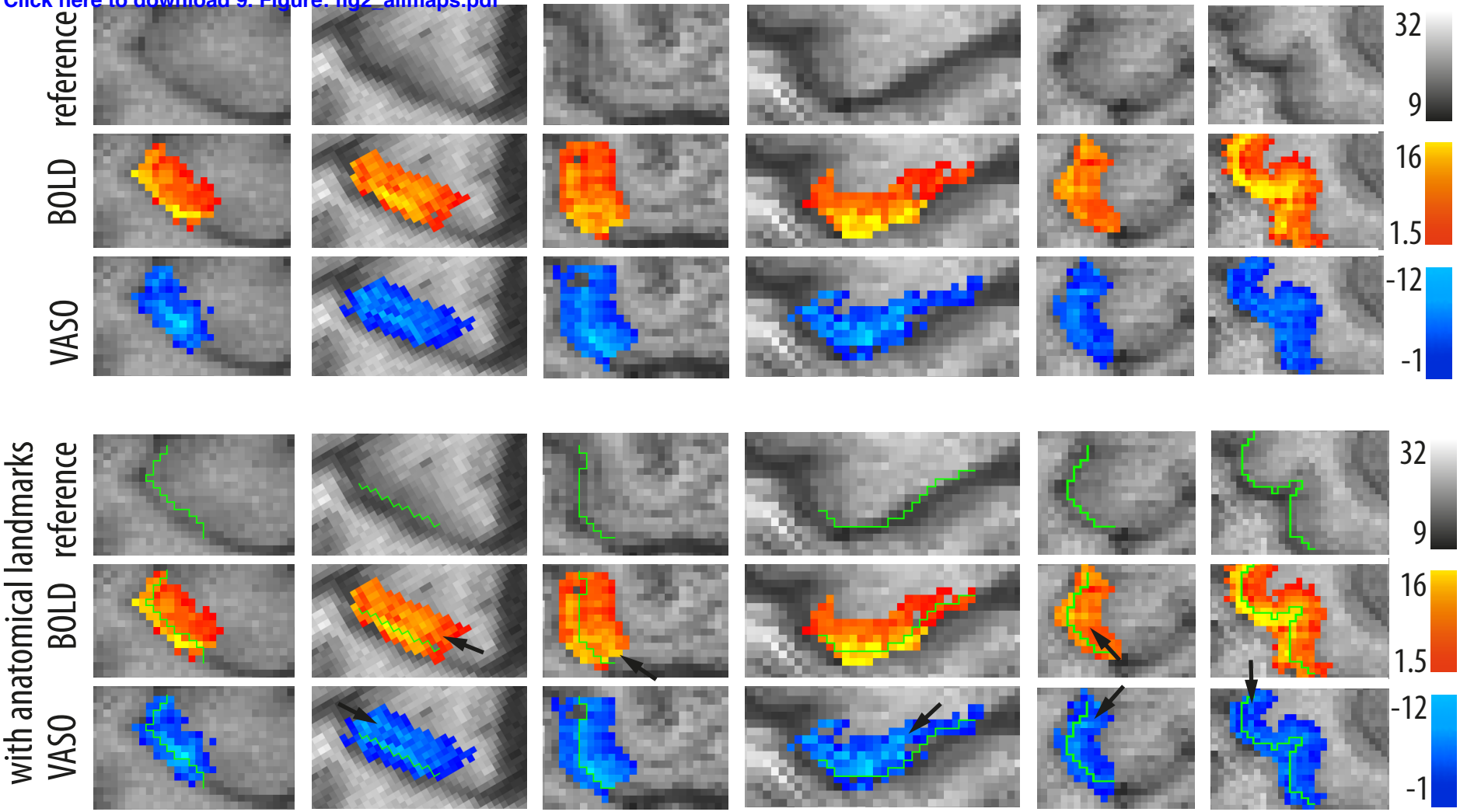

9. Figure
Click here to download 9. Figure: fig3_profiles.pdf

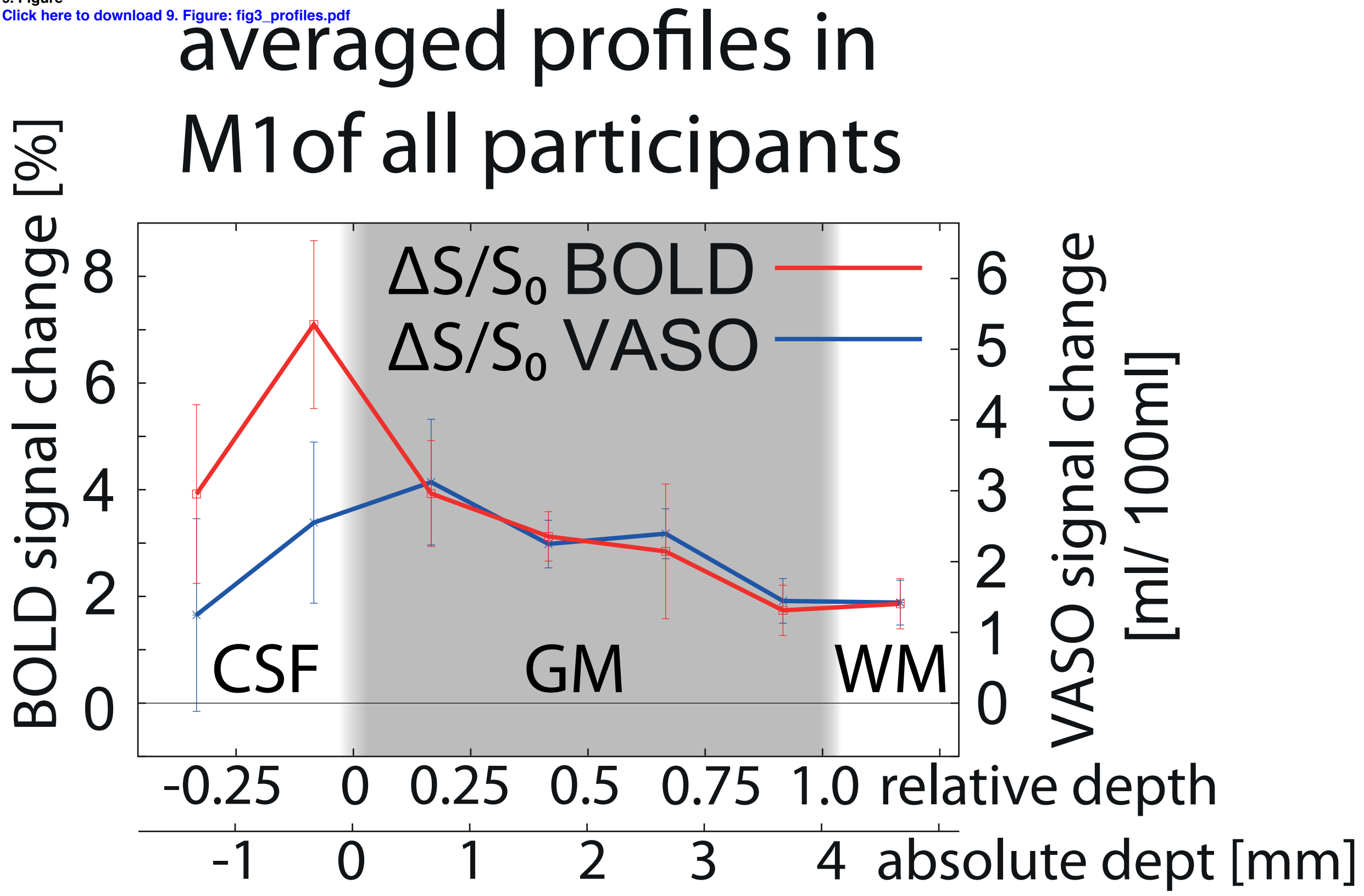

9. Figure

Click here to download 9. Figure: fig4_timecourses.pdf

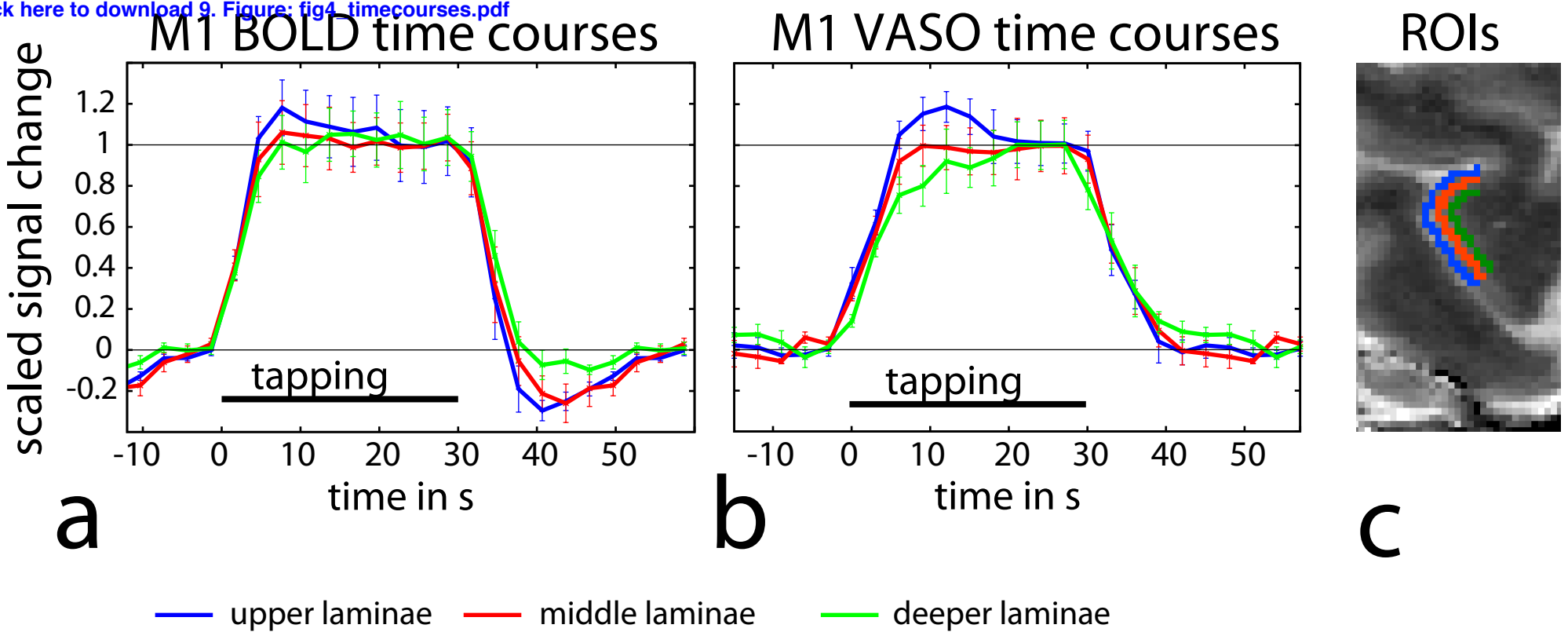

9. Figure
Click here to download 9. Figure: fig5_ipsilateral.pdf

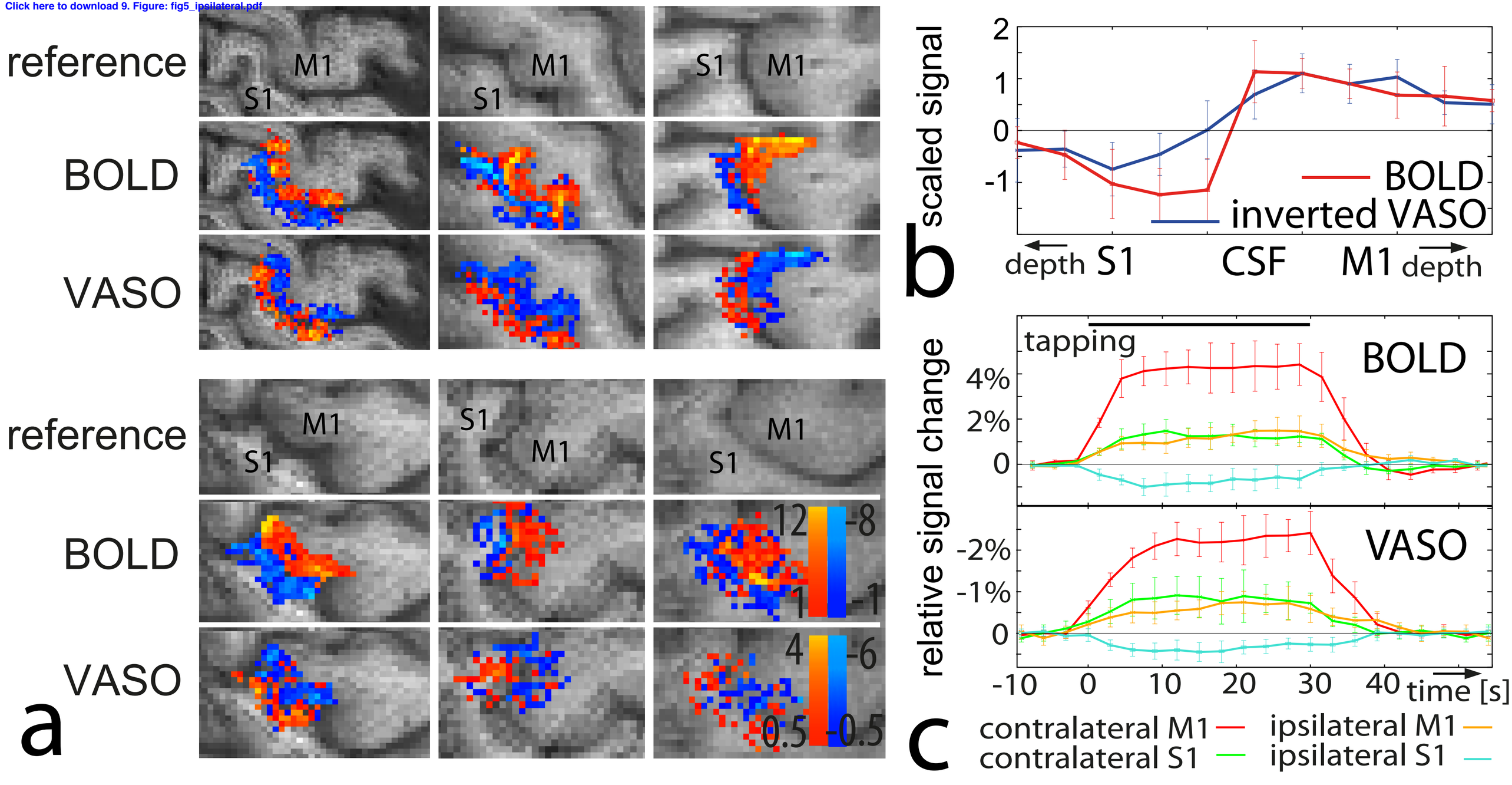

9. Figure
Click here to download 9. Figure: fig6_animals.pdf

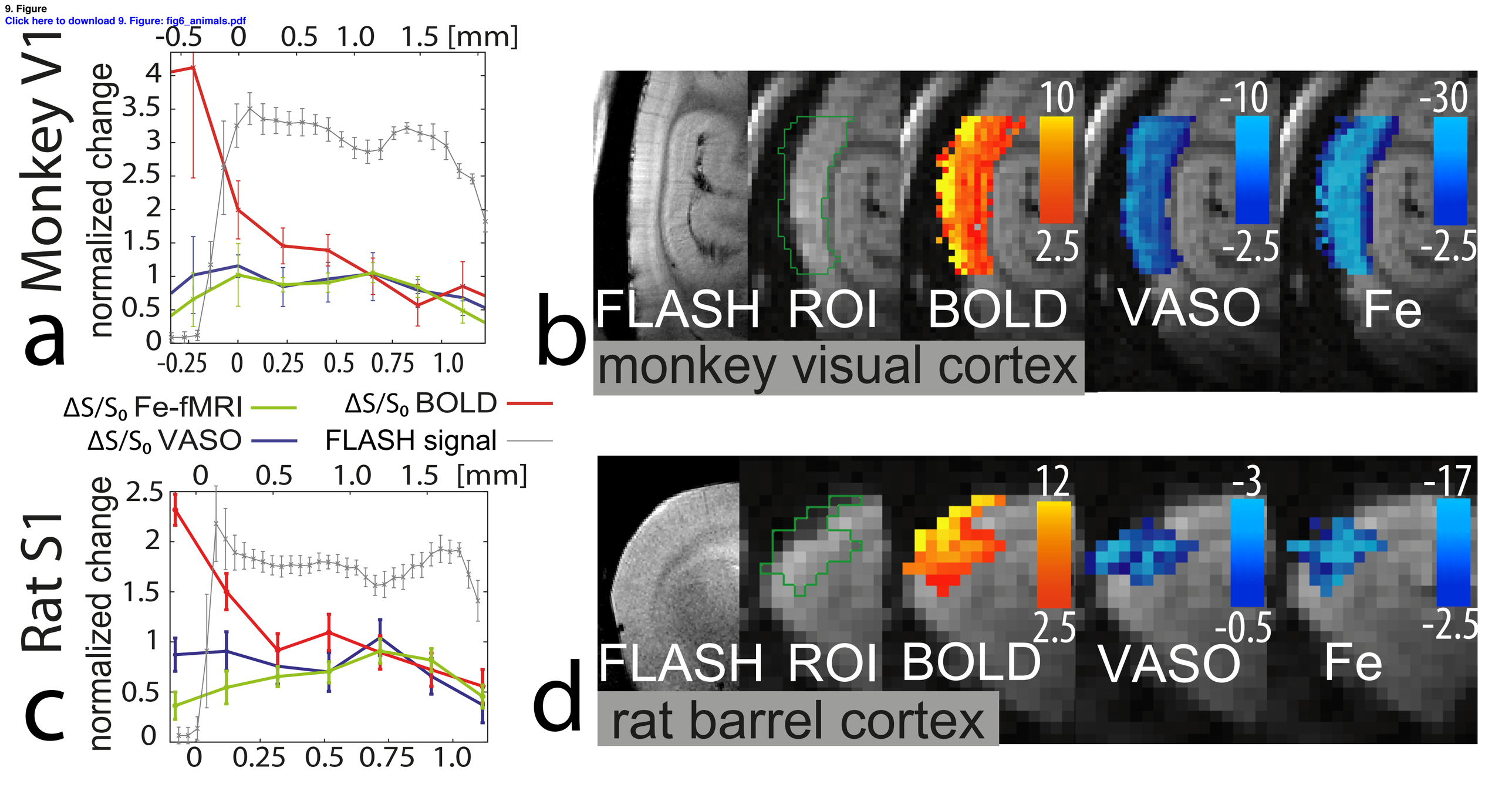

9. Figure

Click here to download 9. Figure: fig7_normalization.pdf

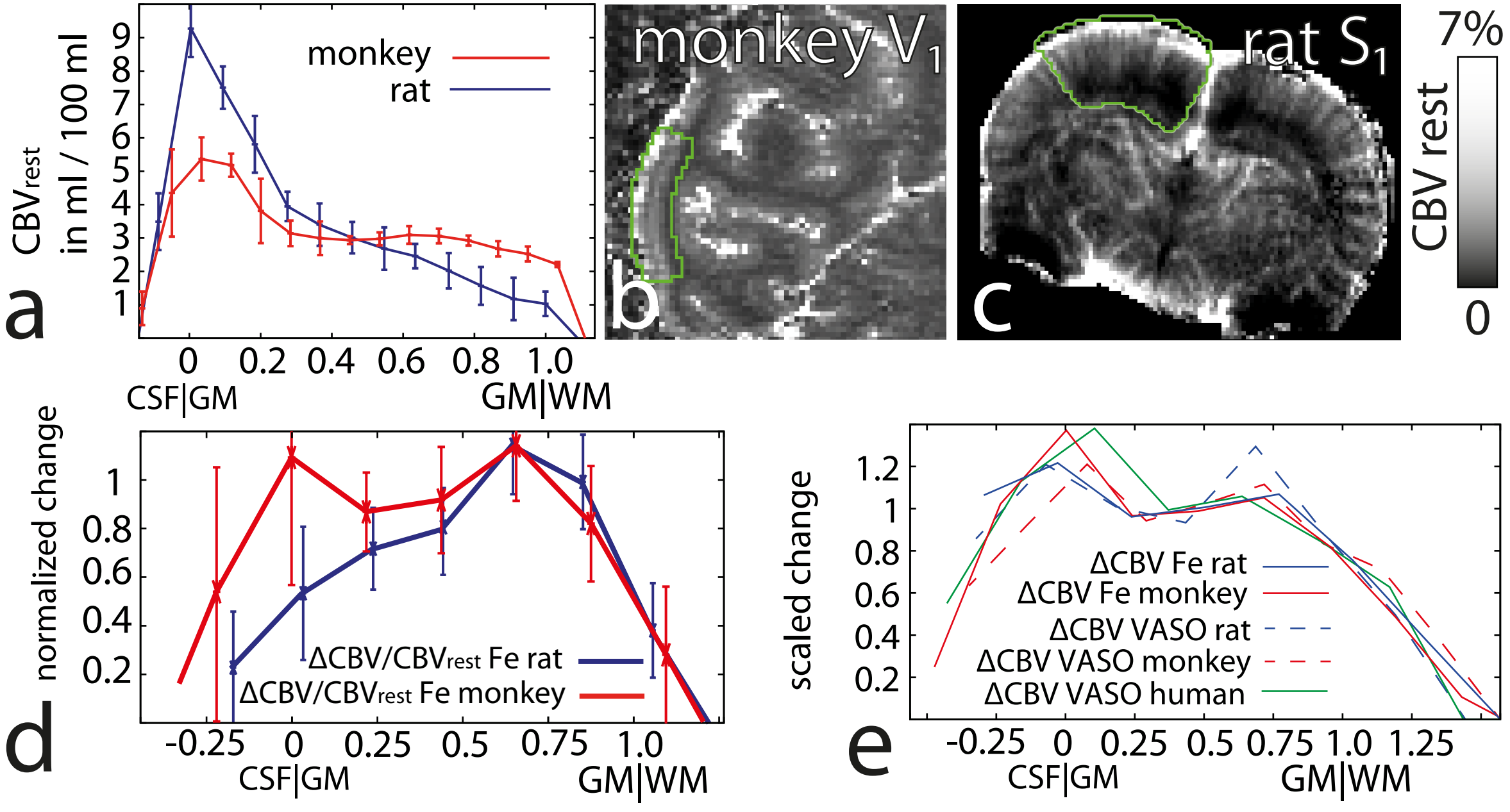

9. Figure

Click here to download 9. Figure_fig3_Interpretation.pdf